Heterodyne holographic microscopy of gold particles.

Michael Atlan,[1] Michel Gross,[1] Pierre Desbiolles,[1] Émilie Absil,[2] Gilles Tessier,[2] and Maïté Coppey-Moisan[3]

[1]*Laboratoire Kastler-Brossel de l'École Normale Supérieure, CNRS UMR 8552,*
Université Pierre et Marie Curie - Paris 6, 24 rue Lhomond 75231 Paris cedex 05. France
[2]*École Supérieure de Physique et de Chimie Industrielles de la Ville de Paris,*
CNRS UPR 5, Université Pierre et Marie Curie - Paris 6,
10 rue Vauquelin 75231 Paris cedex 05. France
[3]*Département de Biologie Cellulaire, Institut Jacques Monod, CNRS UMR 7592,*
Université Paris 6 and 7, 2 Place Jussieu, Tour 43, 75251 Paris Cedex 05. France
(Dated: February 22, 2008)

We report experimental results on heterodyne holographic microscopy of subwavelength-sized gold particles. The apparatus uses continuous green laser illumination of the metal beads in a total internal reflection configuration for dark-field operation. Detection of the scattered light at the illumination wavelength on a charge-coupled device array detector enables 3D localization of brownian particles in water.
OCIS : 180.6900, 090.1995, 170.0180

Assessing microscopic processes by tracking optical labels has a broad range of applications in biology. In particular, monitoring biological phenomena such as cellular-level dynamics is a subject of growing interest. Fluorescent molecules are widely used in this aim, but the observation time of dyes is limited by photobleaching. Quantum dots offer a much better photostability, but they have the inconvenient to blink. Noble metal nanoparticles have the advantage of being perfectly photostable [1]. Originally, light scattered by small metallic particles has been detected in dark field [1] or total internal reflection [2] configuration. To improve the detection sensitivity, interferometric approaches have been introduced [3, 4, 5, 6, 7]. Common-path interference, initially achieved with a Nomarski interferometer [8], translates phase variations into intensity variations, and enables the detection of phase perturbation provoked by spatial [9] or photothermal [10] modulation. Scanning heterodyne detection of the photothermal modulation [3] enables an unmatched combination of sensitivity and selectivity suitable to discriminate particles smaller than 5 nm from their background. Photothermal imaging relies on a spatial scanning of the laser beams to track the index modulation in the neighborhood of the beads; the temporal noise in the incident light leads to spatial noise in the image acquired sequentially [7]. Wide-field detection schemes alleviate such issues, but their sensitivity in optical mixing configurations would not match heterodyne detection on single detectors levels. We propose here a wide-field, shot-noise limited, tunable CCD heterodyne detection technique able to achieve high-resolution, 3D microscopy of gold particles with a laser source at rates compatible with biological dynamics. The experimental setup is sketched in fig. 1(a).

The main laser beam ($\lambda = 532$ nm, field E_L, 50 mW, single axial mode, CW) is split with a polarizing beam splitter (PBS) in local oscillator (LO) and illumination arms (fields E_{LO} and E_I). A $\lambda/2$ waveplate (HWP),
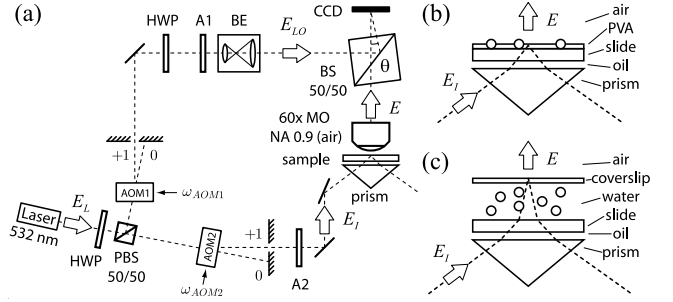

FIG. 1: Experimental setup (a). Evanescent wave illumination of static beads in a plane (b). Total internal reflection configuration for dark-field illumination of beads in a tridimensional environment (c). Acronyms defined in the text.

and neutral densities (A1, A2) allow control of the optical power in each arm. Both beams are frequency-shifted around 80 MHz by acousto-optical modulators (AOM) driven at frequencies ω_{AOM_1}, ω_{AOM_2}. The LO beam passes through a beam expander (BE) to form a plane wave which polarization angle is adjusted with a HWP to maximize the holographic modulation depth. The object is illuminated in dark field configuration by using total internal reflection (TIR). The scattered field $E \ll E_{LO}$ passes through a microscope objective (MO, 60× magnification, NA = 0.9, air). Off-axis optical mixing (θ tilt) of E with E_{LO} with a beam splitter (BS) results in a fringe pattern recorded with a CCD camera (PCO Pixelfly QE, 1392 × 1024 square pixels of 6.7 μm, frame rate $\omega_S = 12$ Hz). Proper frequency detuning $\Delta\omega = \omega_{AOM_2} - \omega_{AOM_1}$, and angular tilt θ enable accurate and sensitive phase-shifting off-axis holography [11, 12].

The first samples observed are thin layers of gold beads (diameter $d = 50$ nm to 200 nm) immobilized in a polyvinyl alcohol (PVA) matrix spread by spin coating onto a glass slide. These slides are set onto a prism used to guide the illumination field E_I and provoke TIR at the
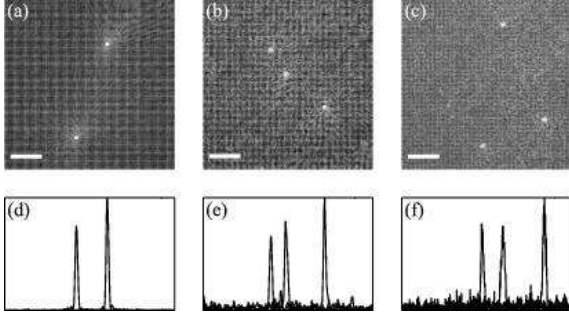
FIG. 2: Squared amplitude holograms $|E|^2$ in logarithmic arbitrary units. 200 nm beads (a), 100 nm beads (b), and 50 nm beads (c). Scale bar is 10 μm. Horizontal profile traces of $|E|^2$ at the beads positions, averaged over 4 pixels (d, e, f), in linear arbitrary units.
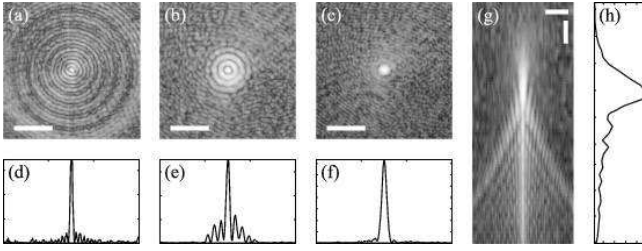

FIG. 3: $|E|^2$ reconstructed images of a 200 nm gold bead with experimental setup of fig.1(b) at several axial positions : $z = 22\,\mu$m (a) $z = 17\,\mu$m (b) $z = 0\,\mu$m (c), displayed in logarithmic arbitrary units. Scale bar is 5 μm. Transverse plane profile traces of $|E|^2$ at the beads positions, averaged over 3 pixels ((d) to (f)), in linear arbitrary units. Axial plane distribution (g) and linear scale profile averaged over 10 pixels in the lateral direction (h).

PVA-air interface. Microscope immersion oil between the prism and the slide enables refractive index matching. The evanescent wave locally frustrated by the beads is turned into a propagative scattered field E collected by the MO. To make E and E_{LO} in phase opposition from one frame to the next, two-phase detection ($\Delta\omega = \omega_S/2$) is performed. Exposure time is $\tau_E = 50$ ms, and holograms are obtained by making the difference of consecutive frames.The complex field $E(x, y, z)$, in the beads plane z, is reconstructed by numerical Fresnel transform [11].

Fig.2 shows the bead images (a,b,c), and the corresponding intensity profiles along x (d,e,f). The images are obtained by averaging ($|E(x, y, z)|^2$) over 4 sequences of 2 images. The beads diameters are 200 (a,d), 100 (b,e) and 50 nm (c,f). Under 50 nm the coherent parasitic light scattered by dust or surface roughness prevents the beads to be distinguished. Fig.3 shows, for 200 nm beads, the x, y images (a,b,c) and the x profiles (d,e,f), at $z = 0$, 17, and 22 μm relative reconstruction distances. It also shows the x, z image (g) and the z profile (h), in the $z = 0$ to 47 μm range. Because the bead emitters are
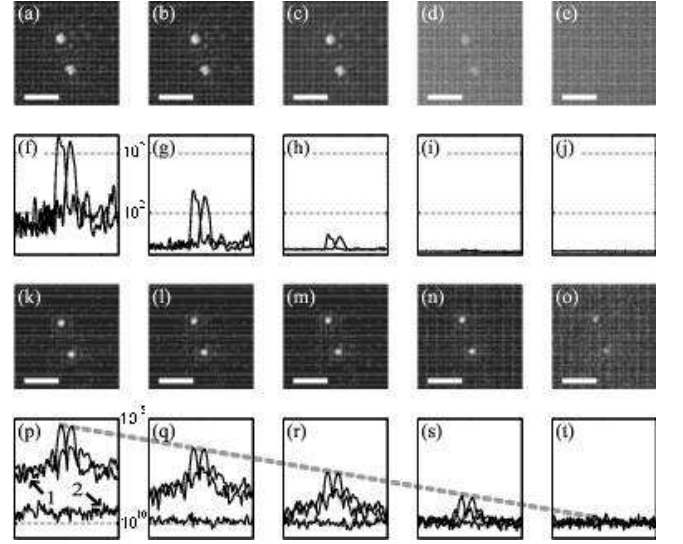

FIG. 4: Intensity images calculated from 4×2 camera frames data of a pair of 200 nm particles. (a) to (e) : direct image (LO beam is off). (k) to (o) : holography (LO beam is on). Scale bar is 5 μm. Illumination field power attenuation ranges from 10^0 to 10^4. Bead profiles without (f) to (j), and with LO beam (p) to (t). The vertical axis range (A.U.) is the same for (f) to (j), and (p) to (t).

close to a plane dielectric interface [13], one observes an asymmetric signal in the z direction of $\sim 7\,\mu$m width at half maximum with rings in the x, y plane. Similar rings have been observed with quantum dot emitters [14, 15]. Quantitative study of this effect [13, 16], is out of the scope of this letter.

To illustrate the sensitivity of our holographic setup, we have displayed on Fig. 4 images ((a, ..., e) and (k, ..., o)) and profiles ((f, ..., j) and (p, ..., t)) of 200 nm beads at different illumination intensities. The illumination beam ($|E_I|^2$) is attenuated by a factor 10^0 (a,f,k,p), 10^1 (b,g,l,q) ..., 10^4 (c,j,o,t). The LO beam is either off (direct imaging : (a, ..., j)), or on (holographic regime : (k, ..., t)). The beads are imaged with much better sensitivity with the LO beam, since the bead signal remains visible by reducing the illumination power over 4 orders of magnitude. Moreover, the signal is proportional to illumination (dashed line throughout Fig.4(p) to (t)). We must note that, at high illumination level (p), the bead detection dynamic range is limited by the parasitic light background (arrow 1) which is several orders of magnitude larger than the holographic detection noise floor (arrow 2), obtained in a cut from the off-axis quietest region of the reconstructed image, away from the beads region. The noise floor (about 10^{10} A.U.), which is related to shot noise of the LO beam, gives an absolute calibration of the bead peak (5×10^{14} A.U. on (k)), since it corresponds to 1 photo electron (e) per pixel [12]. Without attenuation (k), the bead peak area is about 20×20 pixels (see (p)); it corresponds thus to $\sim 2 \times 10^7$ e. One watt of
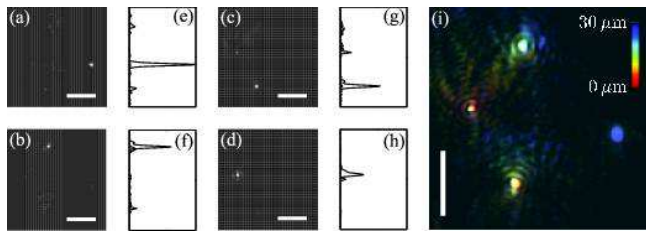
FIG. 5: Axial exploration of a 200 nm gold beads suspension in water. $|E|^2$ images reconstructed 10 μm apart (a) to (d). Linear scale profiles averaged over 4 pixels (e) to (h). Composite image (i). Scale bar is 5 μm.

laser yields $\sim 10^{19}$ photons per second. With 10 mW and $2\tau_E = 100$ ms (2 frames to make an hologram), we get 10^{16} photons. The Mie scattering cross section of 200 nm gold particles (refractive index : $n = 0.39 - 2.38j$ at 532 nm; with $j^2 = -1$) [17] is $0.1\mu m^2$. The total illumination area is ~ 1mm^2. Thus we get 10^9 scattered photons per bead. Since the bead is located at an air-glass interface, most of the light (85%) is scattered within the glass [18], and 1.5×10^8 photons are scattered forward within a 2π solid angle. The collection solid angle of a NA = 0.9 objective is $\sim \pi/4$. We then get 4×10^7 photons on the CCD yielding an expected signal of 2×10^7 e (50% quantum efficiency at 532 nm), in agreement with the experiment.

To assess imaging performances in experimental conditions compatible with biological microscopy, we have performed axial sectioning of dynamic beads; we have imaged a suspension of 200 nm beads in brownian motion in water (see Fig.1(c)). A $\sim 30\,\mu$m-thick layer sample is realized within a slide / parafilm (TM) / coverslip stack. The parafilm layer was heated until melting to serve as waterproof spacer of ~ 30 microns thickness. In this configuration, the top interface (coverslip-air) is the one where TIR occurs. The part of the illumination field E_I not diffracted by the beads undergoes TIR while the scattered field E passes through the MO and is used for imaging. Since the exposure time is short : $\tau_E = 1$ ms, the LO power is increased to fill the CCD dynamic range. Over a time τ, brownian particles travel by a distance $r(\tau) = (6D_B\tau)^{1/2}$, where $D_B = 2.1 \times 10^{-12}$ m^2.s^{-1} is the diffusion coefficient of a 200 nm particle in water. During one exposure, this travel is smaller than the particle size: $r(1$ ms$) \sim 110$ nm. 200 nm beads thus appear to be quasi immobile, but travel from one image to the next by $r(80$ ms$) \sim 1\,\mu$m. This property is used for signal demodulation. The hologram is obtained by subtracting from the current recorded frame the time average of the 10 next consecutive frames. In this way the holographic information is recorded in one exposure $\tau_E = 1$ ms. To localize smaller beads, the exposure time might be shortened accordingly.

Fig.5 shows a series of images (a,b,c,d) and profiles (e,g,f,h) calculated from a single hologram. Images (a) to (d) and profiles (c) to (h) are calculated at axial positions z (a,e), $z + 10\,\mu$m (b,f),... $z + 30\,\mu$m (d,h). A composite image (i) is made from reconstructed intensity holograms at axial positions (z) coded in color in the 30 μm range. The attached multimedia file shows the video rate motion of the particles in this composite image.

In this letter we have performed full field imaging of gold nano particles in 3D at video-rate with exposure times as short as 1 ms. Our holographic technique, which benefits from heterodyne gain, exhibits optimal detection sensitivity, and, since the signal can be easily calibrated, we have verified its agreement with the expected signal. In the future, better axial resolution might be obtained by using the phase of the holographic data. Low-coherence light sources might be used to reduce the background light component and improve depth-sectioning. The background might also be reduced by a selective modulation (e.g. spatial or photothermal) of the particles.

Contact author : atlan@lkb.ens.fr

[1] S. Schultz, D R. Smith, J.J. Mock, and D.A. Schultz. *Proc. Nat. Ac. Sciences*, 97:996, 2000
[2] C. Sonnichsen, S. Geier, N. E. Hecker, G. von Plessen, J. Feldmann, H. Ditlbacher, B. Lamprecht, J. R. Krenn, F. R. Aussenegg, V. Z.-H. Chan, J. P. Spatz, and M. Möller. *Appl. Phys. Lett.*, 77:2949, 2000
[3] D. Boyer et P. Tamarat, A. Maali, B. Lounis, and M. Orrit. *Science*, 297:1160, 2002
[4] K. Lindfors, T. Kalkbrenner, P. Stoller, and V. Sandoghdar. *Phys. Rev. Lett.*, 93:037401, 2004
[5] M.A. van Dijk M. Lippitz, and M. Orrit. *Phys. Rev. Lett.*, 95:267406, 2005
[6] F.V. Ignatovich and L. Novotny. *Phys. Rev. Lett.*, 96:013901, 2006
[7] V. Jacobsen, P. Stoller, C. Brunner, V. Vogel, and V. Sandoghdar. *Optics Express*, 14:405, 2006
[8] J. S. Batchelder and M. A. Taubenblatt. *Appl. Phys. Lett.*, 55:215, 1989
[9] J. Hwang and W. E. Moerner. *Opt. Comm.* , 280:487, 2007
[10] S. Berciaud, D. Lasne, G.A. Blab, L. Cognet, and B.Lounis. *Phys. Rev. B*, 73:045424, 2006
[11] M. Atlan, M. Gross, and E. Absil. *Opt. Lett.*, 32:1456–1458, 2007.
[12] M. Gross and M. Atlan. *Opt. Lett.*, 32:909–911, 2007.
[13] W. Lukosz and R.E. Kunz. *J. Opt. Soc. Am.*, 71:744, 1981.
[14] M. Speidel A. Jon and E.L. Florin. *Opt. Lett.*, 28:69–71, 2003.
[15] D. Patra, I. Gregor, J. Enderlein, and M. Sauer. *Appl. Phys. Lett.*, 87:101103, 2005.
[16] J. Mertz *J. Opt. Soc. Am. B*, 17:1906–1913, 2000.
[17] http://omlc.ogi.edu/calc/mie_calc.html

[18] X. Brokmann, E. Giacobino, M. Dahan, and JP Hermier.
Appl. Phys. Lett., 85:712, 2004.